Pergamon

Int. J. Solids Structures Vol. 34, No. 2, pp. 153–176, 1997
Copyright © 1996 Elsevier Science Ltd
Printed in Great Britain. All rights reserved
0020-7683/97 $15.00 + .00

PII: S0020-7683(96)00008-X

WRINKLING BEHAVIOR OF RECTANGULAR PLATES UNDER LATERAL CONSTRAINT

J. CAO and M. C. BOYCE
Department of Mechanical Engineering, Massachusetts Institute of Technology, Cambridge, MA 02139, U.S.A.

(*Received* 1 *December* 1995; *in revised form* 4 *January* 1996)

Abstract– Wrinkling (buckling) during a sheet forming process is a major consideration when designing part shape, die geometry and processing parameters. In most instances, the sheet metal is constrained to some extent between binders and/or matching dies at some stage during processing. In this paper, we will examine the wrinkling behavior of both elastic and elastic-plastic sheet subjected to edge compression and lateral constraint. A criterion for wrinkling under such constraint is established using a combination of finite element analysis and energy conservation. Various methods of incorporating imperfections into a finite element model in order to capture buckling and post-buckling behavior are discussed. A simple and practical form of imperfection for predictive modeling of buckling is given along with a discussion of the sensitivity of the solution to the magnitude and distribution of imperfections. Using the proposed form of imperfection, we are able to accurately simulate the wrinkling behavior under complicated boundary conditions in a predictive manner. Copyright © 1996 Elsevier Science Ltd.

1. INTRODUCTION

Material and structural instability phenomena such as localization and buckling are major issues to be addressed in designing part shape, die geometry and forming parameters of sheet metal forming, where localization leads to tearing failure of the part during processing and buckling alters the ability to impose stretching during processing and also adversely affects final part appearance, assembling and function. Computational prediction of the onset and growth of these instabilities has significant ramifications for optimizing the design of parts, selecting materials and improving part formability. In this paper, we will focus on the buckling instability of sheet under laterally constrained conditions which are typically encountered during forming (Fig. 1).

Hill's general theory of bifurcation and uniqueness (Hill, 1958) built a foundation for much of the research on buckling since that time. Hutchinson (1974) detailed the bifurcation theory for structures where the material is in the plastic range. An application of the theory to the case of forming under constrained conditions, where lateral constraints (constraint normal to the plane of the sheet) are present in the form of binder/sheet/die or die/sheet/die interactions, was given by Triantafyllidis and Needleman (1980). They applied the bifurcation theory to an annular plate subjected to axisymmetric radial tension along its inner edge. By resting the annular plate on a continuous linear elastic foundation, that is, $\dot{p} = -k\dot{u}_z(r, \theta)$, where the spring constant k is related to the binder stiffness K, they treated the binder as a deformable binder and obtained the effect of binder stiffness on the critical buckling stress and the wave number. Their results were found to compare favorably with the simple beam model of Senior (1956) for the cases where $K = 0$. Also, small strain deformation was assumed. A similar eigenvalue approach for elastic rectangular plates on a non-linear unilateral elastic foundation can be found in recent literature such as Elisakoff *et al.* (1994) and Shahwan *et al.* (1994) whose work was directed towards understanding the buckling of films bonded to a substrate.

For complicated geometry and boundary conditions, numerical solutions using the Finite Element Method have become a prime tool to predict buckling behavior. Although the onset of buckling can be predicted by performing eigenvalue analysis, the highly nonlinear nature of the post-bifurcation behavior makes an analytical solution nearly impossible to obtain (Tomita, 1994). In fact, the post-buckling behavior must be traced by

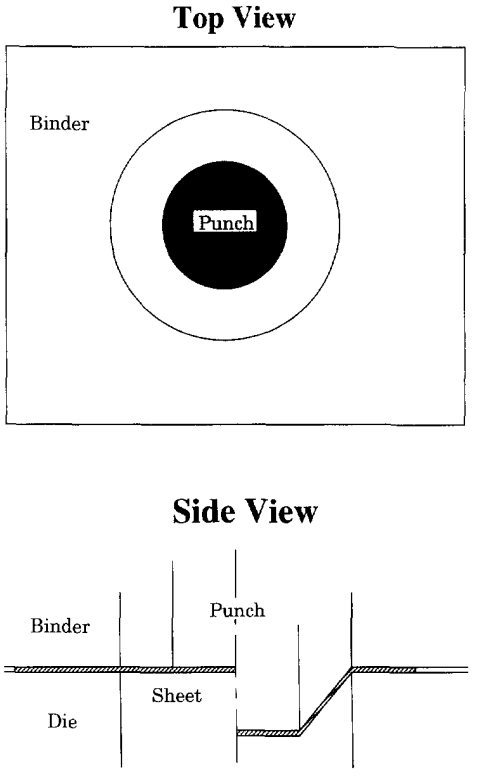

Fig. 1. Schematic of an axisymmetric sheet metal forming process. Here, radial draw-in produces a compressive hoop stress state in the flange section of the sheet which is subjected to the lateral constraint of the binder and the die.

a model with initial imperfection. Most analytical and numerical models implement a specific modal shape or Fourier series in order to capture post-buckling behavior (Triantafyllidis *et al.*, 1980, Fatnassi *et al.*, 1985 and recent proceedings of NumiForm 1992 and Numisheet 1993). For an accurate solution, the correct mode shapes must be known *a priori*. Therefore, obtaining the correct post-buckling mode usually requires several attempts where various frequencies are tried. For a complicated sheet metal forming process, it is not desirable to utilize such a technique due to the relatively long CPU time for each simulation where it would also necessitate an eigenvalue analysis at each increment to determine buckling initiation.

In this paper, we first present our approach in Section 2 for determining the conditions required for a plate to wrinkle† under lateral constraint where the binder and the die are treated as rigid surfaces, which is often the case in practical situations. The criterion specifies the combination of in-plane compressive stress and binder pressure (normal to the plane of the sheet) constraint needed to initiate the wrinkling as well as the mode/wavelength of wrinkling produced and can be easily used with large deformation theory, any constitutive law and hardening law, etc. Numerical verification of modal buckling under lateral constraint is given in Section 3 where imperfections in sinusoidal modal shapes are used in the finite element models. A sensitivity study of the imperfection is presented as well. In order to overcome the shortcoming of using a pre-defined modal imperfection, a simplified imperfection form is presented in Section 4 and compared to our buckling criterion. In Section 5, a robust and simple format for implementation of imperfections into a finite element model is presented which can capture initiation and post-buckling behavior in a predictive manner. Finally, in Section 6, simulations of longer plates under lateral constraint are conducted to study the effect of boundary conditions on the initial buckling stress.

† Sheet buckling in sheet metal forming is generally referred to as wrinkling.

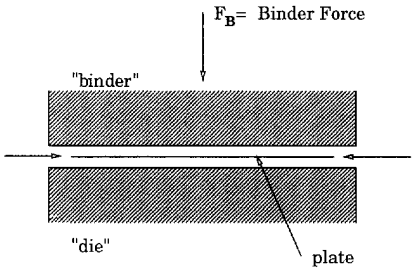

Fig. 2. Schematic of a plate under edge compression and lateral constraint.

2. BUCKLING CRITERION FOR BUCKLING UNDER LATERAL CONSTRAINT

As a basic element in sheet metal forming processes, a portion of the blank is constrained by a die and a binder; then, together with friction, the binder constraint determines the material flow into the deformation zone, the so-called die cavity (Fig. 1). As the punch advances and deforms the sheet, material is drawn into the forming cavity and a compressive stress develops in the plane of the sheet. This compressive stress will result in wrinkling if the binder force is not sufficient to suppress the out-of-plane displacements. This common phenomenon can be simplified to the problem of a rectangular plate subjected to in-plane compression under lateral constraint shown in Fig. 2. The plate is simply supported along the edges at $x = 0$ and $x = L$. If the binder force is zero, the critical stress needed to initiate buckling in the elastic plate is given by [e.g., Timoshenko (1961)]:

$$\sigma_{cr_n} = n^2 \frac{\pi^2 E}{12(1-\nu^2)}\left(\frac{t}{L}\right)^2 = n^2 \sigma_{cr_1} \quad n = 1, 2, \ldots \tag{1}$$

where E is the elastic tensile modulus, ν is Poisson's ratio, and n corresponds to the mode of buckling. The buckling stress σ_{cr_1} is smallest when $n = 1$ (one-half sine wave) and, therefore, mode 1 is the favored mode of buckling. However, if mode 1 is somehow suppressed due to a constraint, then mode 2 wil be favored and so on. Numerous cases of buckling under constraint have been examined, perhaps one of the earliest is a bar on an elastic foundation (e.g., Hartog, 1952, Timoshenko, 1961). These studies show that the critical stress and mode of buckling depend on the level of constraint imposed by the elasticity of the foundation. A more contemporary example is the buckling activated delamination of a thin coating from a substrate (Argon *et al.*, 1989) where the debond energy is computed based on knowledge of the in-plane stress and buckling wavelength. Below, a criterion for the initiation and mode of buckling for a plate sandwiched between a rigid die and a rigid binder is developed in terms of the in-plane compressive stress and the binder pressure normal to the plane of the plate. A combination of finite element analysis and energy conservation is used to construct this criterion.

Finite element model

The plate is modeled with finite strain 4-node reduced integration shell elements† (ABAQUS type S4RF) using a commercial finite element code ABAQUS. This shell element provides a linear interpolation of both displacement and rotation over the element. The reduced integration element has five integration points through the thickness, all located at the center of the element; hourglass controls on displacement and rotation are achieved through modeling an artificial stiffness associated with the zero-energy deformation modes (hourglass modes) which become possible due to the effect of reduced integration on the transverse shear behavior. The finite element code uses an implicit solver where equilibrium is converged upon in each increment using a Newton-Raphson method. As is known, buckling initiates from some form of imperfection in the structure which can be a geometric imperfection (such as lack of flatness), a material imperfection (e.g., non-uniform thickness,

† Shell elements are chosen due to their efficiency in capturing bending and stretching; shell elements are also very effective in modeling sheet metal forming.

weak spots), or loading imperfection (e.g., off-center loading). The geometric imperfection has been commonly modeled by a Fourier series expansion of initial deflection (Timoshenko, 1961, Tennyson, 1970), and a material imperfection modeled by weak elements having either thinner thickness and/or lower yield stress. In the simulations of this section, the form of imperfection is chosen to be a geometric imperfection which positions the mid-surface of the plate to a sinusoidal mode shape ($z_o = At_o \sin n\pi x/L$) of a very small maximum amplitude $A = 0.001$, where n is the buckling mode, t_o is the plate thickness and L is the plate length. Incorporation of the imperfection in this manner acts to predefine the mode obtained; a new method is given later which acts to define the mode in a predictive way.

We begin with an elastic plate of length L, arbitrary width w, thickness t_o, elastic tensile modulus E, and Poisson's ratio ν to illustrate our approach. The plate is modeled with 48 elements along the length (x direction) and one element along the width (y direction) (see Fig. 4). The solution is later generalized to plates of arbitrary length. All rotations of nodes at $y = w$ are set to be identical to those of their counterparts at $y = 0$. Several cases will be examined: a perfect plate (no imperfections), and four plates containing imperfections with the mid-surfaces predisposed to modes 1, 2, 3, and 4, respectively. In all cases, the loading condition consists of a monotonically increasing compressive displacement u_x of edges at $x = 0$ and $x = L$. The stress states of the elements and the total strain energy of the sheet are then recorded as functions of edge displacement u_x.

Criterion

In the case of the perfect elastic plate, buckling does not occur and the plate is therefore under a state of uniform compression. The total strain of this plate, $\mathscr{E}_o$, is simply the elastic strain energy due to uniform uniaxial compression and is normalized by Young's modulus $E*$Volume and shown as a function of normalized displacement (u_x/L) in Fig. 3 (solid curve). The plate pre-positioned to mode 1 is found to undergo mode 1 buckling as expected. The numerically predicted initial buckling stress is nearly identical to the analytical solution σ_{cr_1}. The normalized total strain energy density for the mode 1 buckled plate, $\mathscr{E}_{w_1}/EV$, as a function of edge displacement u_x/L is cross-plotted with that of the perfect plate in Fig. 3 as the dashed line. Similarly, plates buckling in higher modes n were simulated using models with the corresponding sinusoidal imperfection modes n and the total strain energies $\mathscr{E}_{w_n}$ are recorded (Fig. 3).

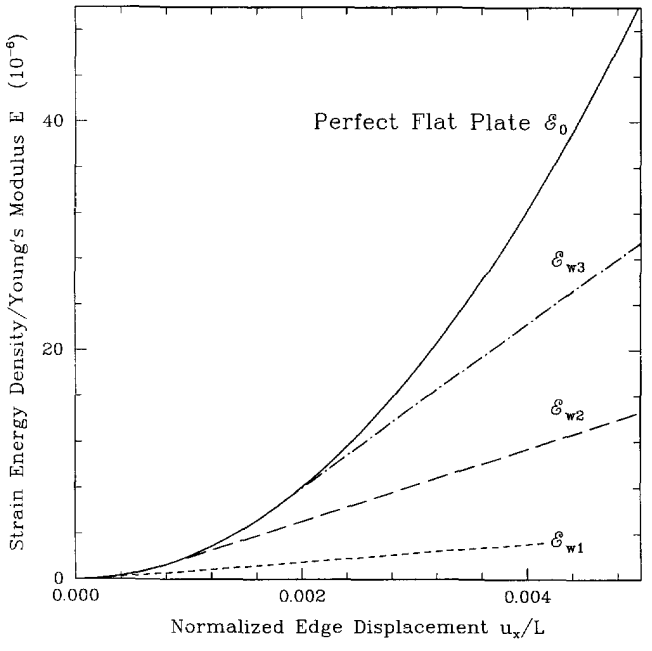

Fig. 3. Total strain energy densities stored in the flat plate and the plates buckling in mode 1, 2 or 3.

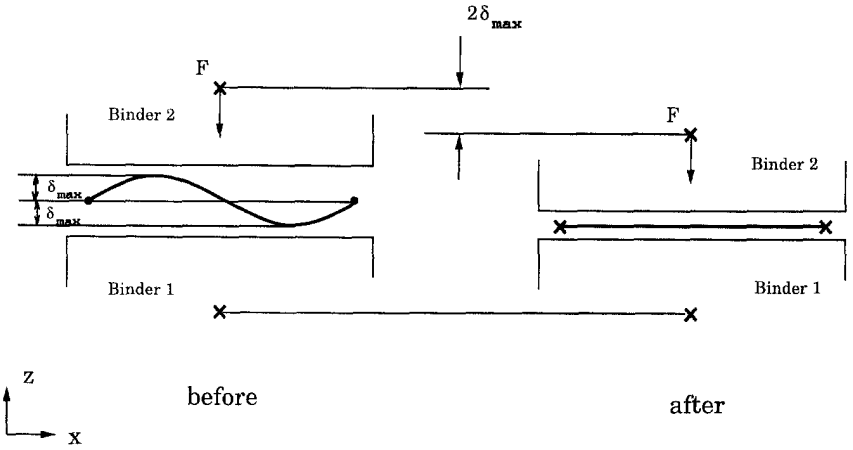

Fig. 4. Schematics of a mode 2 buckled plate being suppressed by the binder.

As shown in Fig. 3, the strain energy of a buckled plate is consistently lower than that of the perfect plate at a certain edge displacement. Note that in the case of coating delamination, this energy difference is taken to be the debonding energy (e.g., Argon *et al.*, 1989). In the case of sheet forming, the difference between the two energies at any given displacement u_x is the external work required to suppress buckling imposed by the binder:

$$\mathscr{W}_n = \mathscr{E}_o - \mathscr{E}_{w_n} = f_n(u_x) \tag{2}$$

where n denotes the buckling mode. Figure 4 shows a plate which was prebuckled in mode 2 due to a compressive displacement $2u_x$ and no lateral constraint which produced a maximum center deflection $2\delta_{max}$. The plate is now placed between two rigid binders and the boundary conditions are set such that the edge displacements of the sheet are fixed in the x direction ($\mathrm{d}u_x = 0$, at $x = 0, L$). Binder 1 is fully constrained while Binder 2 is monotonically displaced $2\delta_{max}$ in the negative z direction.

The total work $\mathscr{W}$ contributed by F is

$$\mathscr{W} = \int_0^{2\delta_{max}} wF\,\mathrm{d}u_z \tag{3}$$

where w is the plate width. An example of the binder reaction force-displacement trajectory is shown in Fig. 5 for the case of a plate prebuckled in mode 2 by an edge compression of $u_x/L = 1/60$. Furthermore, assuming that the relationship between the binder reaction force F and the binder displacement u_{bz} is a second-order polynomial function, that is,

$$F = a(u_{bz} - \delta_{max})^2 + b \tag{4}$$

and denoting F_{max} as the maximum force, we obtain

$$a = -\frac{F_{max}}{\delta_{max}^2}$$

$$b = F_{max}$$

As shown in Fig. 5, eqn (4) fits the behavior extremely well. This agreement is found to hold for higher order modes as well by sampling the press down process at various end displacements and buckling modes. The work $\mathscr{W}$ can then be written as

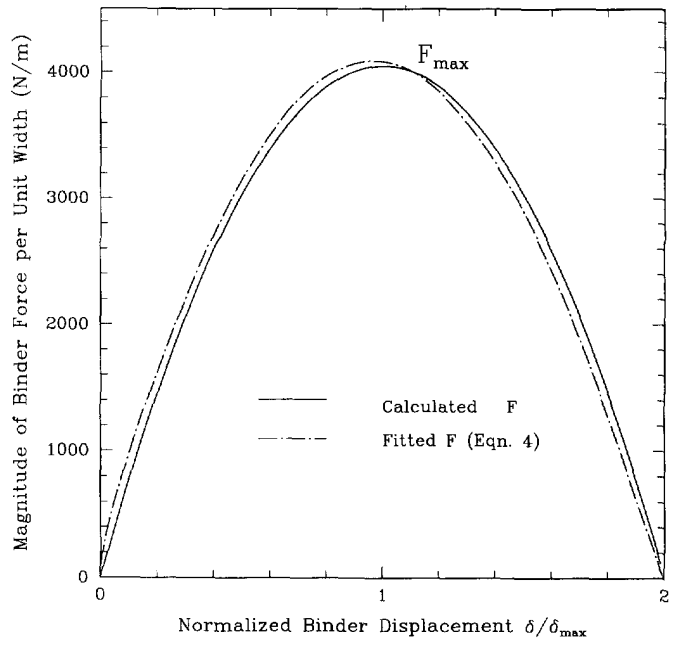

Fig. 5. The trajectories of the binder force per unit width which acts to suppress the mode 1 wrinkling vs the normalized binder displacement for the case of $u_x/L = 1/60$.

$$\mathscr{W} = \tfrac{4}{3}F_{max}\delta_{max}w \tag{5}$$

Combining eqn (5) and eqn (2), we can obtain the maximum force per unit width F_{max_n} as

$$F_{max_n} = \frac{3}{4}\frac{\mathscr{E}_o - \mathscr{E}_{w_n}}{\delta_{max_n}w} \tag{6}$$

or

$$p_{max_n} = \frac{3}{4}\frac{\mathscr{E}_o - \mathscr{E}_{w_n}}{\delta_{max_n}Lw} \tag{7}$$

where p is the effective binder pressure and p_{max_n} is interpreted as the binder pressure needed to suppress buckling of the nth mode at a given u_x/L.

In summary, the binder pressure p_{max_n} needed to suppress mode n wrinkling as a function of edge displacement u_x/L can be calculated by buckling plates and recording the corresponding $\delta_{max}(u_x)$ and $\mathscr{E}_w(u_x)$; then eqn (7) is used together with the energy differences from Fig. 3 to compute p_{max_n}.

Figure 6 shows the calculated p_{max_1} and p_{max_2} as a function of u_x/L. The two curves are found to cross over each other at a specific point, the transition pressure p_{12}, which is the binder pressure where the favored mode of buckling transits from mode 1 to mode 2. For example, consider the case of a binder pressure p^* applied on the plate, the plate would buckle in mode 1 and mode 2 at displacements of u_1^* and u_2^*, respectively. For the case where $p^* < p_{12}$, we have $u_1^* < u_2^*$ (Fig. 6), i.e., the critical buckling stress for mode 1 is lower than that for mode 2, and therefore, the plate would favor mode 1. On the other hand, for the case $p^{**} > p_{12}$, we have $u_2^{**} < u_1^{**}$, and therefore, the plate would buckle in mode 2.

This criterion thus quantitatively defines the critical buckling stress and, also, the mode of buckling which will occur in the presence of a given binder pressure. For a limited plate length L, mode n buckling corresponds to a wavelength of L/n. Therefore, a relationship between the normalized wavelength (λ/t) and the pressure (p/E) for a plate of length L can be defined as the dash-dotted line in Fig. 7. Now, considering an infinite plate which can

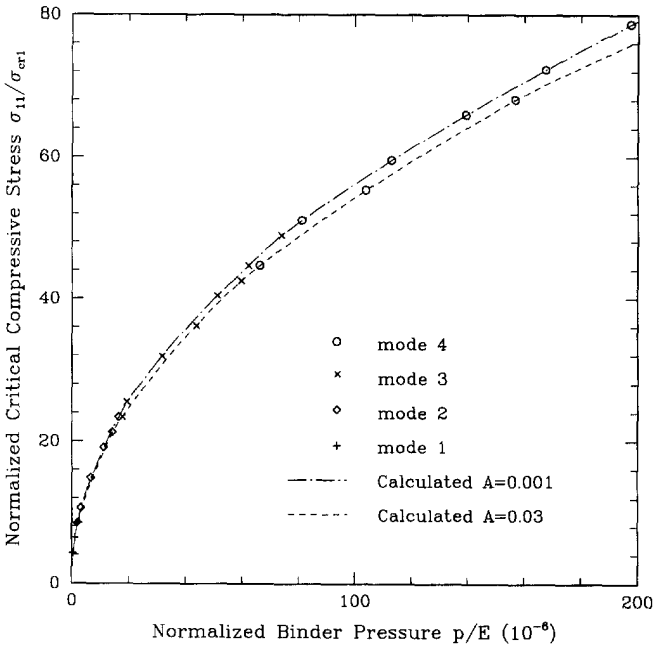

Fig. 8. Calculated critical buckling stress as a function of applied normal pressure for an elastic plate.

$$\sigma_{cr} = E * \ln \frac{2 \min [u_1, u_2, u_3, \cdots]}{L},$$

where E is Young's modulus, u_n is the edge displacement of mode n at a binder pressure of p. The dash-dotted line in Fig. 8 shows the calculated critical buckling stress vs the normalized applied pressure obtained from the analysis of both the finite plate (which has limited mode shapes, but whose buckling stress will differ with pressure) and the infinite plate. Earlier, Cao and Boyce provided a similar relationship (buckling stress vs binder pressure) based on a combination of their numerical simulations and experiments of aluminum cup forming under various constant binder force conditions (see Jalkh *et al.*, 1993). They utilized the relationship to optimize the forming process by increasing the binder force during the process only when it was needed to suppress wrinkling. Figure 8 demonstrates the ability to analytically obtain such curves for use in designing forming process parameters without need for experimental data.

Note that the mode and critical stress criteria shown as the dash-dotted curves in Figs 7 and 8 were obtained with a maximum offset amount A set at 0.001. However, the buckling stress level is sensitive to the level of imperfection. For example, for a plate whose mid-surface is pre-positioned to mode 2 via $z_o = At_o \sin(2\pi x/L)$, subjected to edge compression only, $A = 0.001$ predicts the buckling stress to be $4\sigma_{cr_1}$ (excellent agreement with the analytical solution), while $A = 0.03$ predicts $3.88\sigma_{cr_1}$. The simulated buckling stress decreases as the magnitude of the imperfection increases. However, we note that imperfections of $A > 0.03$ are not physically realistic. As a result of the imperfection sensitivity, the force required to suppress the buckling will also vary with the level of imperfection. Figure 9 shows the correlation of the normalized maximum offset A and the transition pressure p_{23} between modes 2 and 3 normalized to maximum p_{23} obtained. For the elastic material, we notice that this relationship is almost linear. To illustrate the imperfection sensitivity in the other modes, the dash-dotted curves in Figs 7 and 8 which defined the buckling wavelength and the buckling stress as a function of p, respectively, are calculated when A is 0.001, while the dashed curves define the relationship when A is 0.03. The offset is found to affect the transition pressure between modes (Fig. 7), but does not strongly influence the overall length of the critical buckling stress (Fig. 8).

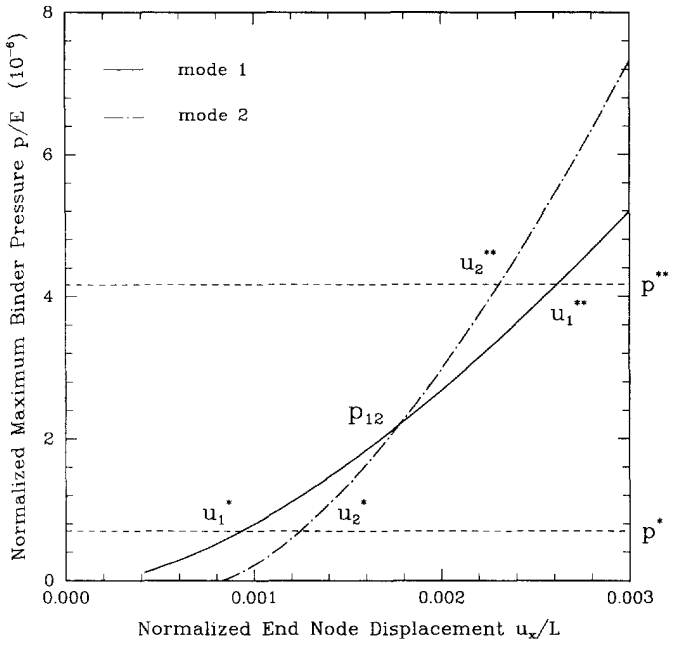

Fig. 6. Maximum binder pressures as functions of the end node displacement for the first and second mode buckling.

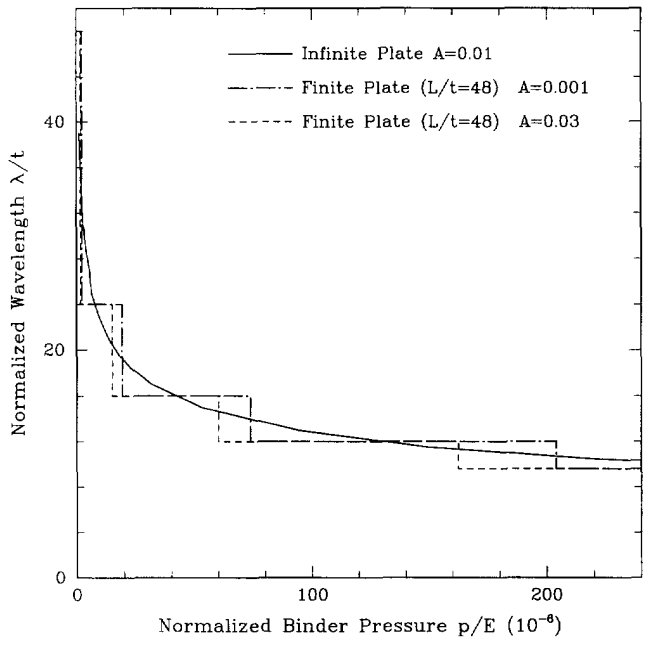

Fig. 7. Calculated buckling wavelength as a function of applied normal pressure for an elastic plate of Young's modulus E and thickness t.

buckle into any wavelength, a continuous relationship between wavelength and binder pressure is expected to characterize the buckling behavior of a plate under constraint. This can be obtained numerically by continuously performing the above analysis for plates of length $L_1, L_2, \cdots, L_\infty$, where $L_1 < L_2 < \cdots < L_\infty$. The result of the normalized wavelength (λ/t) as a function of lateral pressure (p/E) for the case of an elastic material is shown in Fig. 7 where we observe a decrease in wavelength with increasing binder pressure. The curve shows an extremely nonlinear behavior even for the elastic material.

The critical buckling stress as a function of applied pressure can be calculated as

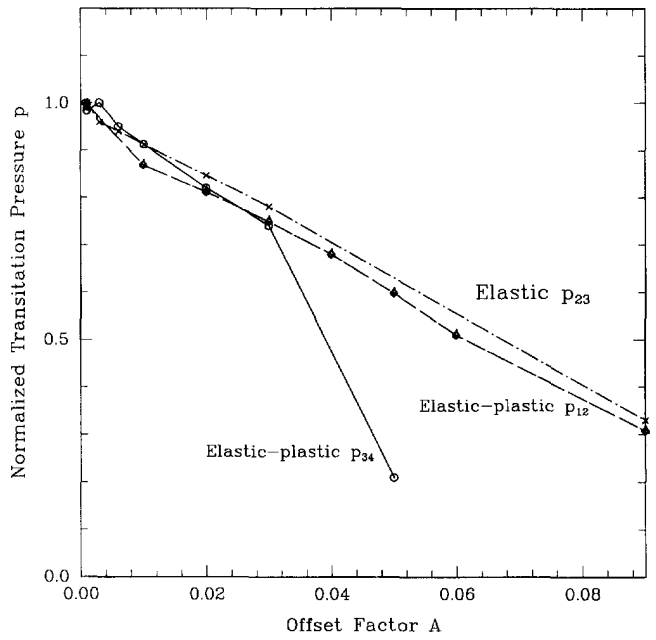

Fig. 9. Normalized transition pressures p as a function of the offset factor A in FEM model ($z_o = At_o \sin(n\pi x/L)$).

Behavior of elastic-plastic plate

In practice, wrinkling failure during forming more typically occurs when the sheet is in the range of plastic deformation. The basic idea of energy conservation presented above for the elastic plate still applies, although the press-down procedure must be interpreted as a virtual process in the case of the elastic-plastic sheet. Here, the calculated wrinkling wavelength and stress as a function of applied pressure and the sensitivity of the solutions to the magnitude of the imperfections implemented into the finite element model will be compared to those obtained for the elastic plate.

The material in our simulations is aluminum Al2008-T4 which exhibits an elastic-plastic stress-strain behavior with plastic behavior characterized by $\sigma = K\varepsilon^n$, where the material strength coefficient is $K = 528$ MPa and the strain hardening exponent is $n = 0.265$; the elastic modulus is $E = 70$ GPa. The plastic behavior of the material is modeled using the isotropic Mises yield criterion with an initial yield stress σ_{Y_o} of 120 MPa and also assuming isotropic strain hardening following the given power law hardening.

A complete curve defining the correlation between the applied lateral constraint p_{binder} (now normalized to the initial yield stress σ_{Y_o}) and the resulting buckling wavelength λ (normalized to the plate thickness t_o) for a finite plate and an infinite plate can be calculated and is shown in Fig. 10. The results are similar to the elastic case (Fig. 7), however, the mode shape transition pressures are at much lower values. Figure 11 shows the calculated critical buckling stress σ/σ_{cr_1} vs the binder pressure p_{binder}/σ_{Y_o}. Notice that the curve is much flatter compared to that of the elastic material (Fig. 8) because of the yielding of the elastic-plastic plate, where the initial yield stress $\sigma_{Y_o} = 4.35\sigma_{cr1}$. Additionally, recent experiments and simulations of conical cup forming of this same material found the cups to wrinkle under the binder in a manner dependent on the binder pressure. The buckling wavelengths and critical stresses obtained in the cup forming experiments are shown in Figs 10 and 11, respectively, showing excellent agreement with the results predicted by the criterion. More details about the cup forming results and the potential applications of our criterion are available in Cao (1995) and Cao and Boyce (1994 and 1996).

As in the case of the elastic material, the results shown in Figs 10 and 11 vary somewhat depending on the amount of the initial geometric imperfection offset A used in the finite element model. The solid and dashed lines in Fig. 9 show the effect of the offset A on p_{34} (the transition pressure between mode 3 and mode 4 for a finite plate having $L/t = 48$) and

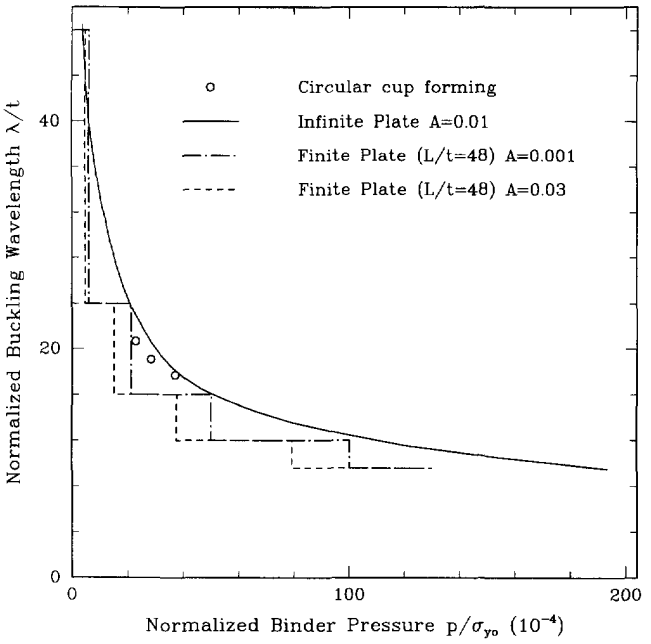

Fig. 10. Calculated buckling wavelength as a function of applied normal pressure for an elastic-plastic material compared with the simulation results of a circular cup forming process.

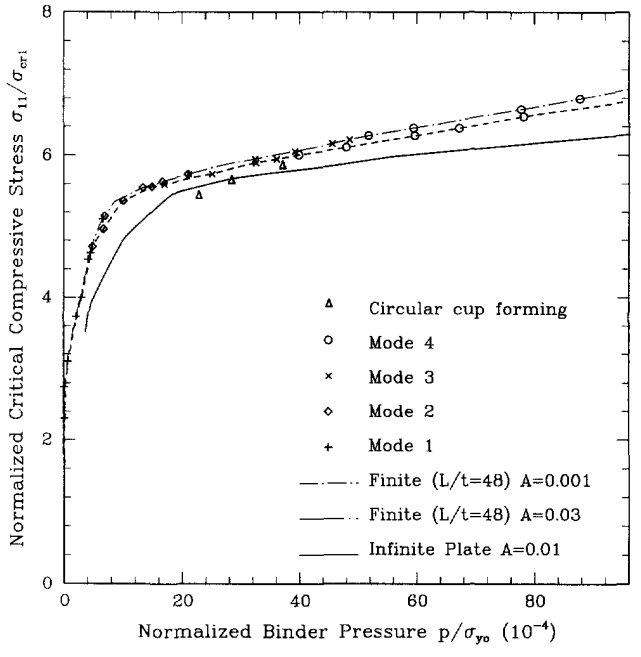

Fig. 11. Calculated critical buckling stress as a function of applied normal pressure together with that obtained from three-dimensional simulations of circular cup forming. Note that the yield stress $\sigma_y 0 = 5.44\sigma_{crl}$.

p_{12} (the transition pressure between mode 1 and mode 2) normalized to the highest value in their corresponding group, respectively. Notice that plastic deformation prior to buckling happens in modes higher than mode 3 and a very different sensitivity phenomenon from the elastic material is found; that is, the solution has a reasonable estimate when $A < 0.03$ and varies significantly when $A > 0.03$. A typical thickness variation in a blank of sheet is approximately $1\% t_o$ and we note that the solution is not that sensitive when realistic values for the imperfection are used. Overall, the solution of the critical buckling stress is more sensitive to the initial imperfection in the plastic range than that in the elastic range. A

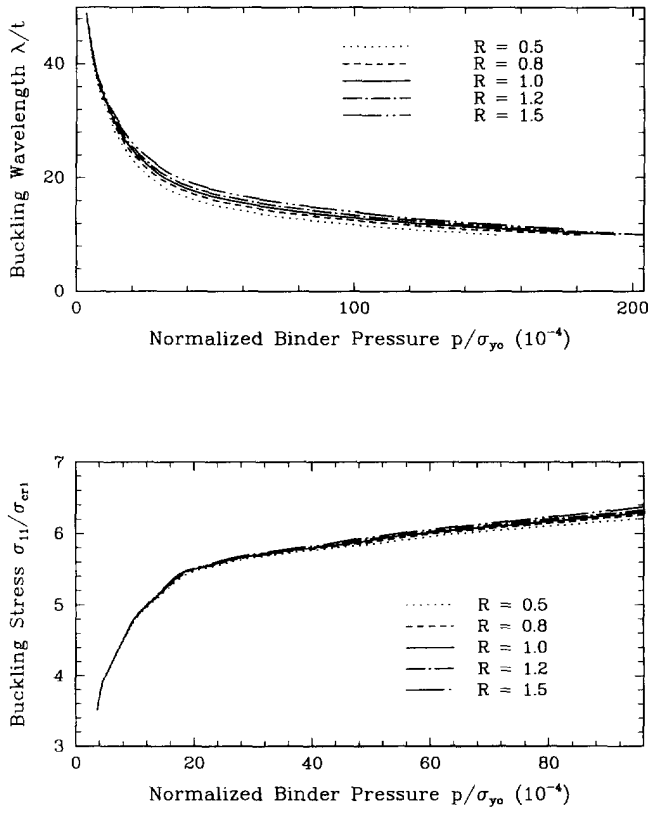

Fig. 12. Effect of the transverse anisotropy ratio R on the wrinkling.

similar result was obtained by Needleman (1975) for the case of buckling of a circular plate subjected to in-plane compression only. In the remainder of this paper, we will choose $A = 0.01$ as our reference except when specified otherwise.

The plasticity of aluminum sheet is generally anisotropic and often characterized by the R ratio, the ratio of the width to thickness strain in a uniaxial tension test. Figure 12 illustrates the effect of the normal anisotropy parameter, R, on wrinkling by plotting the buckling wavelength and initial buckling stress as a function of applied binder pressure. The yield criterion used is the 1948 Hill anisotropic yield surface. It can be seen that at a certain pressure, the initial buckling stress increases with the increasing R ratio. This result is consistent with the observation of Triantafyllidis and Needleman (1980) and the dependency is rather small (about 5% for the worst case).

3. SIMULATION OF MODAL BUCKLING UNDER CONSTRAINT

Above, a criterion for determining the relationship between lateral constraint and the buckling mode/wavelength/stress for a rectangular plate using finite element analysis and considerations of energy conservation was given. In this section, a finite element model with a lateral constraint imposed by a binder is constructed to study the accuracy of the buckling initiation and mode predicted by the criterion. Modal buckling of the elastic plate is demonstrated here.

Finite element model

A rectangular plate having $L/t = 48$ is placed between two rigid plates where a normal compressive force is then applied and designated as F_{binder} (Fig. 2). The force provides an initial pressure p_{binder} normal to the plate. The elastic plate is modeled with 48 four-node finite strain reduced integration elements (ABAQUS type S4RF) in the elongation direction. The bottom rigid plate is referred to as the die and the upper plate is the binder. The

interfaces between the two rigid plates and the elastic plate are taken to be frictionless and modeled by a three-dimensional interface element (ABAQUS type IRS4). The two rigid surfaces are originally placed one-half of the sheet thickness apart from the centerline of the plate. An exponential relationship between the contact pressure p and clearance c between the rigid surface and the plate is used to artificially simulate a build-up to material resistance in the z direction.

$$p = p_o \frac{\ln(1-c_o+c)}{\ln(1-c_o)} \quad c < c_o$$
$$p = 0 \quad c > c_o \tag{8}$$

where c_o is set to be one-half of the thickness and p_o is set to be on the order of 10 MPa ($p/E = 1.4\text{E-}4$) which is a typical contact pressure. The contact pressure-clearance relation provides negligible penetration in most instances and eases convergence of the contact solution. The selection of contact pressure will only affect the rate of convergence, but not the final solution as long as negligible penetration is enforced. Note that the through-thickness stress is of no practical concern as it is negligible compared to in-plane stress levels.

The form of imperfection is still taken to be a pre-disposed mid-surface as a sine wave $z_o = At_o \sin(n\pi x/L)$, where A is 0.01. In order to simulate precise first, second and fourth mode buckling, the boundary condition of the sheet is set as $u_z|_{x=0} = u_z|_{x=L}$, and for the third mode, it is further restricted to

$$u_z|_{x=0} = u_z|_{x=L} = \tfrac{1}{4}(u_z|_{x=L/6} + 2u_z|_{x=L/2} + u_z|_{x=5L/6}).$$

The die is fixed and the binder has only one degree of freedom, translation in the z direction. The first step during loading is to apply a constant force on the binder while the elastic plate is fixed in the x and y directions at $x = L/2$ so that the plate will not slide out of the contact area due to the frictionless interface conditions. This dummy boundary condition is removed in the second loading step while the binder force is kept constant and the two edges ($x = 0$ and $x = L$) are then displaced inwards in the x direction.

Results

Results from several simulations are detailed below. The simulations consist of compressing plates predisposed to modes 1, 2, 3, and 4 under various constant binder pressures.

First, plates with mode 1 pre-conditioning (wavelength $\lambda/t = 48$) were compressed under various levels of binder pressure. For all pressures of p_{binder} (normalized by Young's modulus E) less than 2.08E−6, mode 1 buckling was obtained (Figs 13 and 14). It is found that the initial buckling stress levels for $p_{binder} \neq 0$ are much higher than σ_{cr_1} because of the lateral constraint. Also, the post-buckling stress level is higher than σ_{cr_1}. As shown earlier in Fig. 7, once the normalized pressure p_{binder}/E exceeds 2.08E−6, the elastic plate now attempts to buckle in mode 2. However, because of the mode 1 pre-conditioning which does not provide for mode 2 buckling, the numerical simulation could not capture mode 2 buckling. Instead, buckling was not predicted for $p/E > 2.08\text{E}-6$.

In order to capture mode 2 (wavelength $\lambda/t = 24$), the middle surface is pre-positioned as $z_o = At_o \sin(2\pi x/L)$. Simulations show plates buckled in mode 2 when the applied normalized pressure is less than 19.4E−6. Similar to the mode 1/mode 2 transition, the plate favors mode 3 when p_{binder}/E exceeds 19.4E−6. Using mode 3 pre-dispositioning, plates are found to buckle in a perfect mode 3 when $p_{binder}/E \leqslant 72.2\text{E}-6$.

A summary of the above simulations can be clearly outlined by plotting the resulting buckling stress normalized to σ_{cr_1} (Fig. 13) and buckling wavelength (Fig. 14) as a function of the applied binder pressure together with those calculated earlier in Section 2. Excellent agreement is obtained showing the predictive abiility of the criterion given in Section 2.

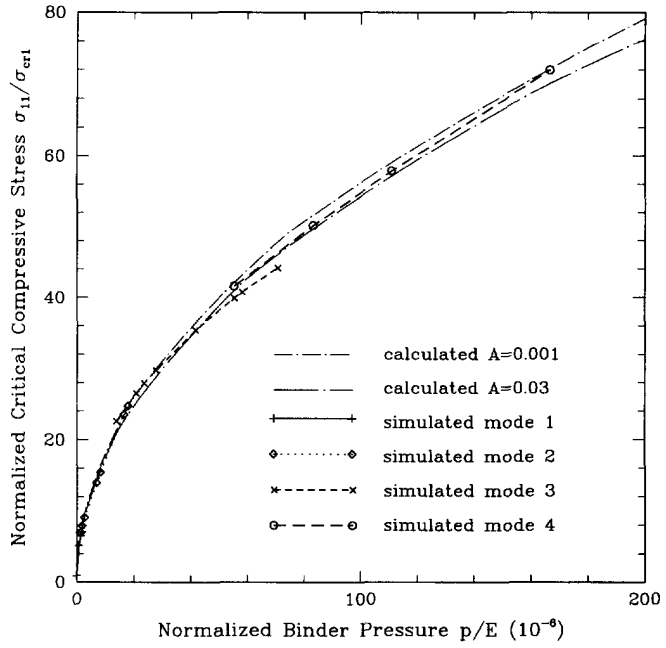

Fig. 13. Critical buckling stress and the associated buckling mode of an elastic plate with mode preconditioning in FEM models subjected to lateral constraint as a function of applied binder pressure compared to the calculated result in Section 2.

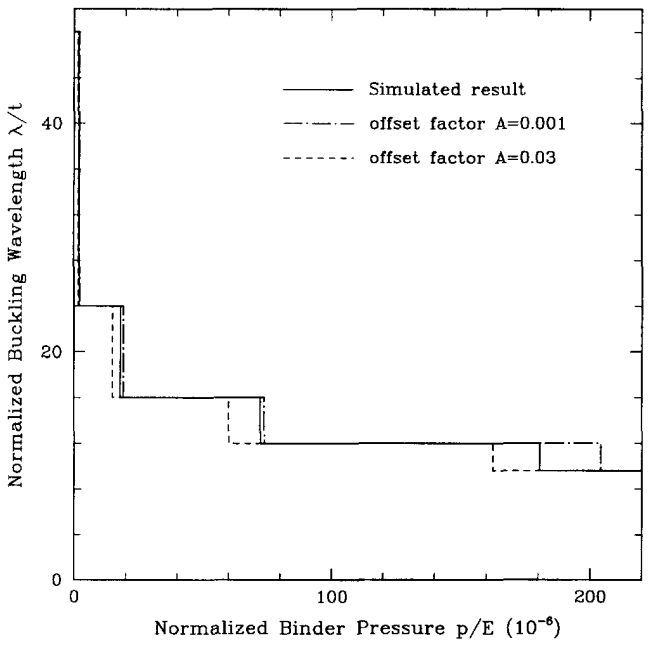

Fig. 14. Calculated and simulated buckling wavelength using mode preconditioning in an FEM model as a function of applied binder pressure for an elastic plate $L/t = 48$.

4. SIMPLIFIED IMPERFECTION FORM AND SENSITIVITY STUDY

To simulate the buckling behavior, some form of imperfection has to be implemented into the finite element model. Above, plates under lateral constraint with pre-conditioned modes (restricted displacement boundary conditions and mode pre-dispositioning imperfection) were simulated. Results were found to match the criterion extremely well. However, in a more typical situation and for a complicated system, the buckling mode is not known *a priori* and it is not guaranteed that the sinusoidal wave imperfection implemented in the model is the correct mode. In order to simplify the incorporation of imperfections and also

to build the basis for the next section where a robust finite element model will be proposed, we examine imperfections in a form of thinned elements with an offset mid-surface representing material and geometrical imperfection, respectively. The sensitivity of the solution to the magnitude of the two parameters (i.e., thinning amount and offset amount) of this new form of imperfection is also examined.

Finite element model

In addition to the previous method which pre-disposes the initial central line into a specific sine wave pattern, we also propose here a new method for incorporating imperfections which is easier and more practical from a modeling/meshing point of view, especially when one moves on to large forming simulations. Several columns of elements are selected to be thinner, $t = (1-f)t_o$ and $f = 0.02$, and with a mid-surface offset, $z_o = At_o$ and $A = 0.01$, in the positive or negative z direction depending on the buckling mode to be captured. Figure 15 shows the finite element mesh of the plate where the scales in x, y and z directions are (1, 1, 100). The shaded areas are thinned plus offset elements. Model A is intended to capture the first and third buckling modes. For capturing the second and fourth modes, the locations and patterns of thinned plus offset elements are changed as shown in Figs 15c and 15d, respectively. All other conditions, i.e., the amount of thinning and the magnitude of the mid-surface offset, are the same as those of model A. In each simulation, the loading and boundary conditions are nearly identical as those in the previous section except that there is no restriction on $u_z|_{x=0}$ and $u_z|_{x=L}$, which is close to practical cases where the plate is constrained between a die and a binder, but is not necessarily simply supported on its edges.

Comparison between the simplified model and the sine wave model

Results for the buckling of elastic plates under in-plane compression, relaxed boundary conditions and two different amounts of lateral constraint are now presented. The finite element model A described above is now subjected to a normalized binder pressure p_b/E of 1.8E-6 and 72.4E-6. The model correctly predicts mode 1 buckling at p_b/E 1.8E-6 and mode 3 bucklng at of 72.4E-6. The results of the mid-surface stress trajectory are shown in Fig. 16 together with that obtained from the models with the pre-positioned sinusoidal shapes. Nearly identical results are obtained demonstrating that the simplified imperfection model is feasible and effective.

Sensitivity to the magnitude of imperfection

Recall that the offset z_o of the neutral axis and the thickness deduction Δt of imperfection sites were set to 1% and 2% of the nominal plate thickness t_o, respectively, in the simulations presented in the previous section. In order to examine the sensitivity of the result to the magnitude of imperfections, the case where the plate is modeled using model B (mode 2) in Fig. 15 and subjected to a normalized binder pressure of $P/E = 5.42\text{E}-6$ is studied. First, the thickness deduction factor f is kept constant at 0.02 while the offset factor A changes from 0.005 to 0.01, 0.02 and 0.03. The resulting normalized critical buckling stresses are shown as the triangles in Fig. 17. As we can see, the stress level decreases as the offset amount A increases. In addition, as in the case where no contact was involved (Section 2), the model with $A = 0$ cannot capture buckling under constraint even in the presence of a thickness deduction showing the importance of offset as a critical aspect in capturing buckling. Secondly, the offset A is taken to be constant at 0.01, while the thinning factor f changes from 0 to 0.02 to 0.04. The normalized critical stresses for this variation are also shown as the circles in Fig. 17. Again, the critical buckling stress decreases as f increases. However, unlike the model with $A = 0$ and $f \neq 0$ which could not predict the buckling behavior, the model with $A \neq 0$ and $f = 0$ was found to predict buckling. Overall, the buckling behavior of the plate under constraint is more sensitive to the geometry imperfection denoted by the offset amount of the neutral axis, than to the material imperfection modeled by the thickness deduction. This can be demonstrated by one more simulation where defects with $A = 0.03$ and $f = 0.06$. The result shown as the upside-down triangle in Fig. 17 is extremely close to the case where $A = 0.03$ and $f = 0.02$.

a: model A view from (0,0,1)

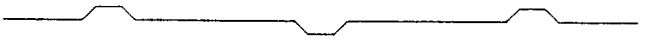

b: model A view from (0,1,0) with a scale of (1.,1.,100.)

c: model B view from (0,1,0) with a scale of (1.,1.,100.)

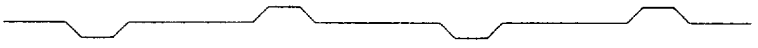

d: model C view from (0,1,0) with a scale of (1.,1.,100.)

Fig. 15. Finite element models of a plate with thinned and offset elements.

5. ROBUST FINITE ELEMENT MODEL

As discussed earlier, the post-buckling behavior requires some form of initial imperfection in order to be captured. In the case of a plate under lateral constraint, modal imperfection, where the mid-surface of the entire plate is set to a certain sinusoidal shape ($z_o = At_o \sin(n\pi x/L)$), would either provide buckling with a wavelength of $\lambda = L/n$ or no buckling. In order to obtain the correct buckling behavior, several cases with various modal imperfections must be simulated in order to obtain the lowest buckling stress which corresponds to the correct buckling mode (Section 3). As an initial step towards constructing a robust finite element model, modal imperfection was replaced by a simplified model of periodically thinning elements and offsetting their neutral axes (Section 4); the periodicity corresponds to modal peaks. The simplified model was found to be effective and provides almost identical results to that obtained from the modal imperfection for the selected tests.

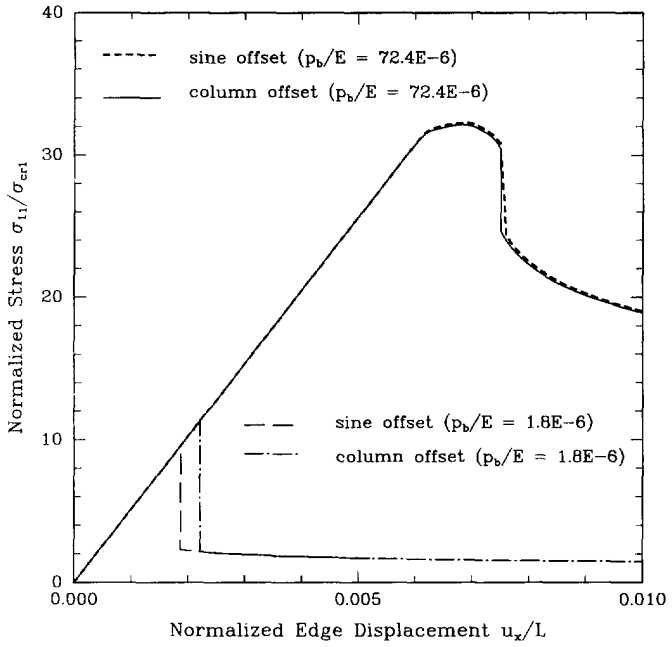

Fig. 16. Trajectories of stress σ_{11} of the middle surfaces of element no. 48 in plates subjected to lateral constraints.

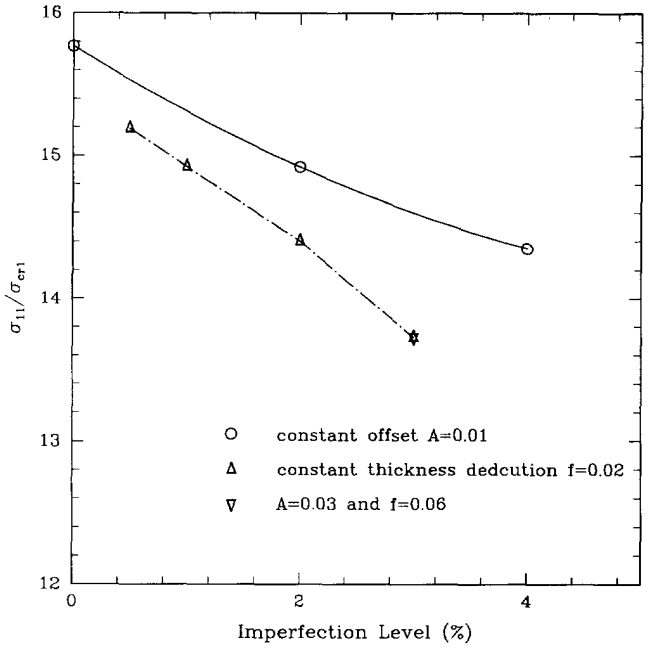

Fig. 17. Sensitivity of normalized buckling stress to the magnitude of the offset A (dash-dotted curve) and thickness deduction f (solid curve) at the case of normalized binder pressure at p_{binder}/E of 5.42E − 6. Note that the y-axis is limited to better show sensitivity.

In this section, we propose a finite element model with randomly distributed imperfections, where imperfections have the same form as presented in the simplified model. The predictive nature of the random distribution model and the sensitivities of the solutions to the distribution of imperfections will be presented.

Finite element model

The basic problem formulation, finite element model and boundary conditions, are identical to those in Section 3 except 96 elements are now used to model the plate and the

a) Model D view from (0,0,1).

b) Model D view from (0,1,0) with a scale of (1.,1.,100.).

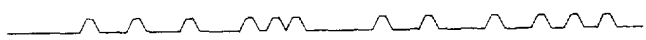

c) Model E view from (0,1,0) with a scale of (1.,1.,100.).

d) Model F view from (0,1,0) with a scale of (1.,1.,100.).

Fig. 18. Finite element models with random distributions of thinned and offset elements.

zero-clearance pressure for the contact problem is set to be 50 MPa to prevent any nodal penetration into the rigid surfaces (binder and die).

Here, the feasibility of using a random distribution of imperfections in a finite element model for the purposes of predicting wrinkling behavior of an elastic-plastic material will be examined. Three random distributions denoted as models D, E and F shown in Fig. 18, where the scales in x, y and z directions are (1, 1, 100), will be examined. In each model, there are 12 "weak" elements (the darkened elements in Fig. 18) out of a total of 96 elements, which account for approximately 12.5% of the area. These weak elements are selected by a random generator and have a thickness deduction factor f of 0.02 and a mid-surface offset factor A of 0.01 in the positive z direction.

Results

The buckling of elastic-plastic plates subjected to in-plane compression and different levels of binder force is now simulated here as described earlier. First, model D is subjected

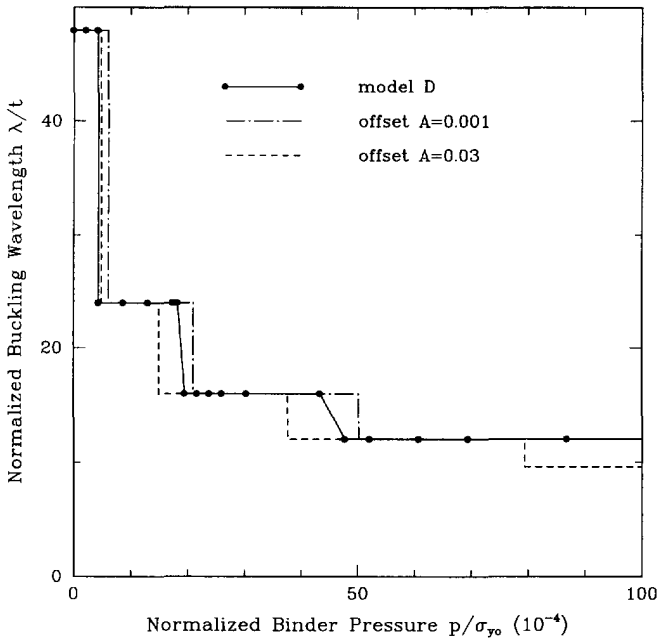

Fig. 19(a). Calculated and simulated buckling wavelength as a function of applied normal pressure for a finite elastic-plastic plate ($L/t = 48$).

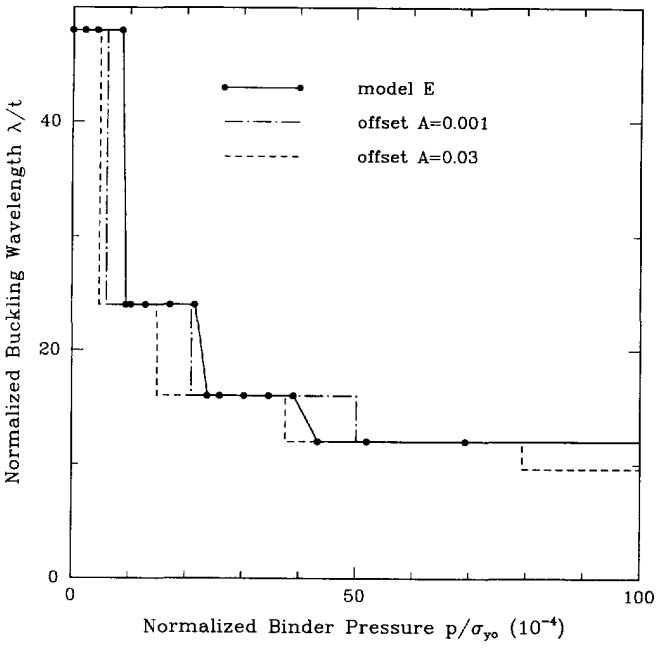

Fig. 19(b). Calculated and simulated buckling wavelength as a function of applied normal pressure for a finite elastic-plastic plate ($L/t = 48$).

to various levels of binder pressure and then compressed in the plane. Simulations predict the plate buckling in mode 1 and capture the post-buckling behavior when $0 < p_{binder}/\sigma_{y_o} < 5.33\text{E}-4$, in mode 2 when $5.33\text{E-}4 < p_{binder}/\sigma_{y_o} < 2.25\text{E}-3$, in mode 3 when $2.25\text{E}-3 < p_{binder}/\sigma_{y_o} < 5.42\text{E}-3$ and in mode 4 when $5.42\text{E}-3 < p_{binder}/\sigma_{y_o} < 1.30\text{E}-2$. Results are compared to the theoretical data obtained in Section 2 and shown in Fig. 19a. Figures 19b and 19c show the simulated buckling wavelength as a function of normalized binder pressure obtained by using models E and F, respectively. The corresponding critical buckling stress as a function of binder pressure together with the calculated result obtained from energy conservation in Section 2 are shown in Fig. 20.

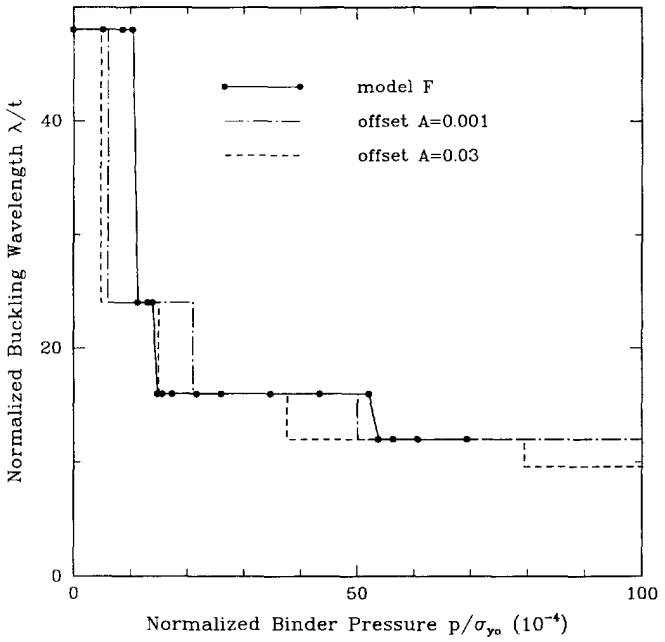

Fig. 19c. Calculated and simulated buckling wavelength as a function of applied normal pressure for a finite elastic-plastic plate ($L/t = 48$).

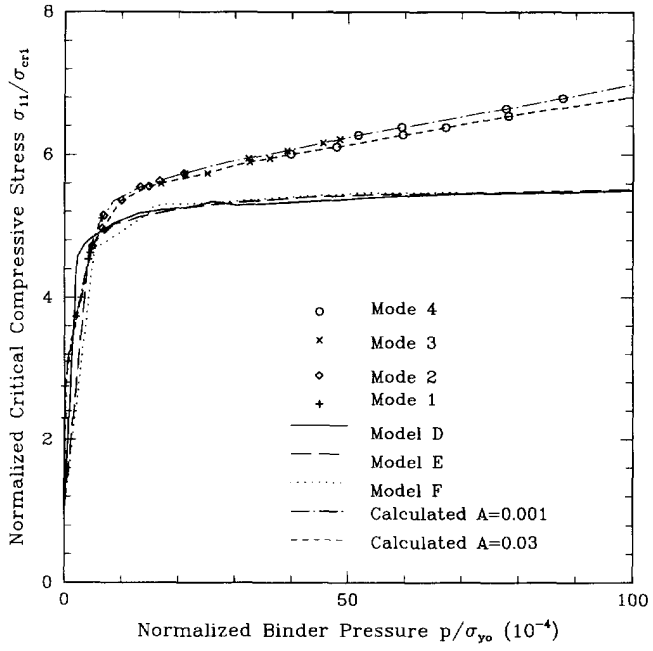

Fig. 20. Calculated and simulated critical buckling stress as a function of applied normal pressure for an elastic-plastic plate.

It can be clearly seen that all three models predict the buckling mode very accurately and provide almost identical critical stress trajectories under various levels of binder pressure. The difference between the simulated and the calculated stress level is because of the difference on the edge boundary conditions (relaxed, with no restriction on $u_z|_{x=o}$ and $u_z|_{x=L}$, vs restricted $u_z|_{x=0} = u_z|_{x=L}$). This will be demonstrated clearly later in Fig. 22.

The simulation results demonstrate the robustness of the finite element model with built-in random distribution of imperfections, which can capture not only the initiation of the buckling but also the post-buckling behavior. The success of the model for the case of the elastic-plastic material is due to the slightly earlier plastic deformation of these offset

elements which takes the plate through to post-buckling, showing the ability to use this approach in a predictive manner for capturing buckling under constraint, i.e., the behavior does not need to be known *a priori*.

6. SIMULATION OF LONGER PLATE BUCKLING UNDER CONSTRAINT

The prediction of buckling modes of plates under lateral constraints obtained by numerical simulations in the previous section agrees with our criterion (Fig. 19) extremely well. However, there exists a difference of initial buckling stress between the calculated and simulated results (Fig. 20). This is due to a combination of relaxed edge boundary conditions and a limited length of the plate. The dependence of critical buckling stress on the length of plates and boundary conditions was also reported by Shahwan and Wass (1994) for the case of buckling of unilaterally constrained elastic rectangular plates. In order to reduce the effect of boundary conditions and further examine the predictive nature of our proposed numerical model, longer plates having a total length three times that of the previous plates ($L'/t = 144$ vs $L/t = 48$) are now considered in this section.

Finite element model

Four various finite element models are used to numerically simulate the buckling of longer plates under lateral constraint. The first two models (Models G and H) have 144 shell elements to model the plate. The third (Model I) and fourth model (Model J) have 192 and 216 elements, respectively. The imperfection is in a form of randomly distributed thinned ($f = 0.02$) elements with an offset ($A = 0.01$) mid-surface. The ratio of number of weak elements to the total number of the shell elements is kept the same as before, that is, 12.5%. Figure 21 shows the side view of the original meshes of these models with a scaling of (1, 1, 100). The models are then subjected to edge compression and a range of binder pressures to study the buckling behavior of longer plates.

Results

The results of numerical simulations will be compared with the calculated wavelengths and buckling stresses of an infinite plate obtained in Section 2. As observed in the previous section, all of the models are capable of capturing various post-buckling behavior. The deformed meshes under several binder pressures using Model G are shown in Fig. 22 as a demonstration. As shown, despite the relaxed edges, the central part of the longer plate is undergoing an almost perfect modal buckling. Therefore, the wavelength of the central plate is taken to be the resulting buckling wavelength under the given binder pressure. For the case of $p_{binder}/\sigma_{y_0} = 4.34\text{E}-3$, the buckling wavelength λ/t is 14.14. Meanwhile, the relaxed boundary conditions results in an 8% lower buckling stress in the 20 edge elements than the other elements. The average buckling stress of the center part of the plate is reported as the buckling stress under that binder pressure. Figures 23 and 24 show the predicted normalized buckling wavelength and initial buckling stress as a function of applied binder pressure using Models G to J. The calculated results obtained in Section 2 are also shown as the solid line in the figures.

All the simulation results have excellent correlation with the calculated results from energy conservation. The wavelength is predicted. Also, the predictions of initial buckling stress are closer to the calculated result than those of short plates (Fig. 20), indicating that the difference of initial buckling stress observed in the previous section is indeed due to the edge effect on the limited length configuration. Similar results are obtained by using finite element Models G to I where the mesh densities are 1.0/mm, 1.0/mm and 1.33/mm, respectively. A better result is obtained when the mesh density is increased to 1.5/mm (Model J). The consistent results obtained from the four various models demonstrate the robustness and predictive nature of our proposed method of modeling imperfections in a practical and easy way.

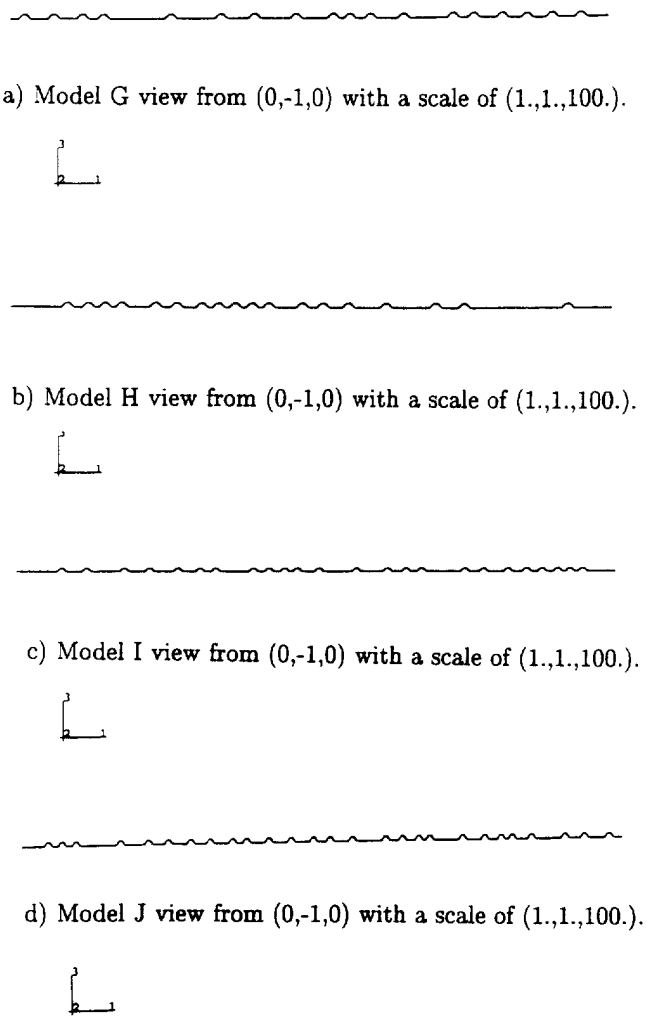

Fig. 21. Finite element models of a longer plate.

7. CONCLUSION

A buckling criterion was developed for a rectangular plate subjected to edge compression and lateral constraint imposed by rigid binders using a combination of finite element analysis and energy conservation law. A perfect plate is initially loaded with edge compression u_x only and its total strain energy $\mathscr{E}_o(u_x)$ is recorded. Plates buckling to various modes are achieved by initial dis-positioning of the middle surface into proper mode shapes. Their associated total strain energy $\mathscr{E}_w(u_x)$ is also recorded. Then the lateral constraint force/pressure needed to suppress wrinkling is calculated based on the energy difference and buckling amplitude δ. The wrinkling criterion then defines the buckling mode/wavelength and the buckling stress as a function of applied lateral constraint for the cases of both elastic and elastic-plastic plates. In order to initiate wrinkling in the numerical simulation, some form of imperfection must be implemented into the finite element model. Finite element models with specified modal imperfection and boundary conditions were subjected to edge compression and lateral constraint to verify our criterion to be accurate. However, as discussed in the text, modal imperfection is not predictive. A simpler, more practical and predictive way of providing this, imperfections in a form of randomly distributed, thinned and offset elements, was developed and used to simulate plate buckling under lateral constraint. The simulations were found to be able to predict the correct buckling mode/stress and to capture the post-buckling behavior and, therefore, demonstrated the robustness and predictive manner of our proposed finite element model. Simulation of plate buckling is found to be somewhat imperfection sensitive, more sensitive to the geometric

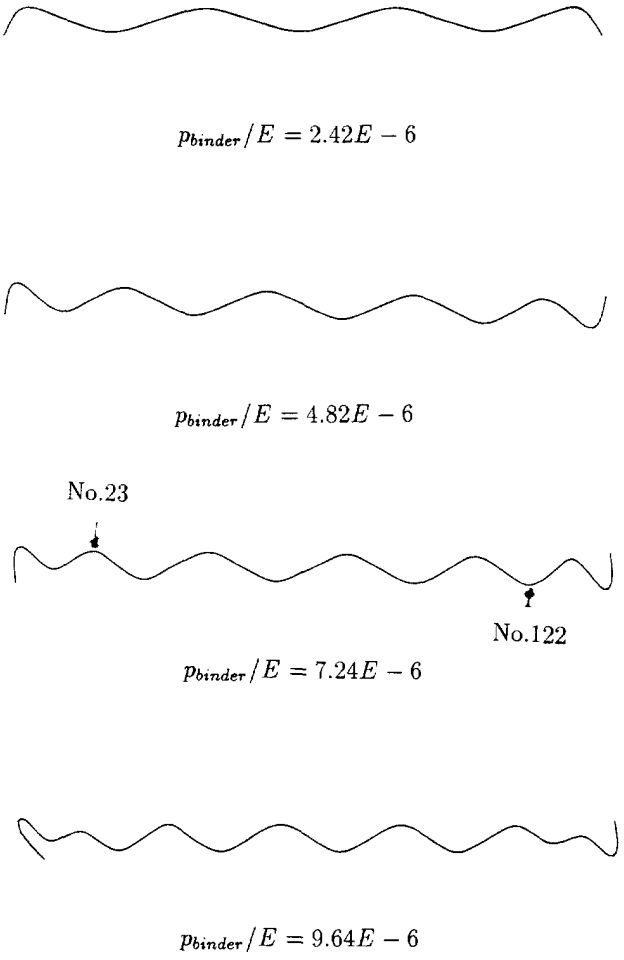

Fig. 22. Deformed plates under various binder pressures using model G.

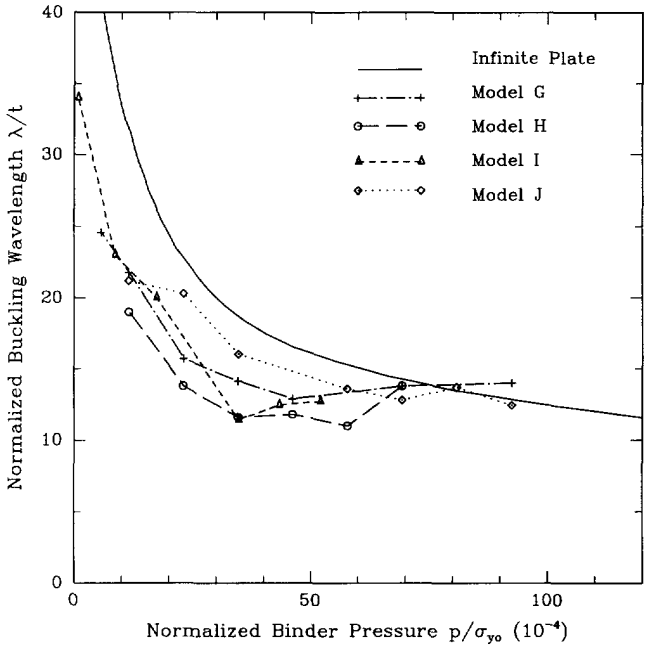

Fig. 23.

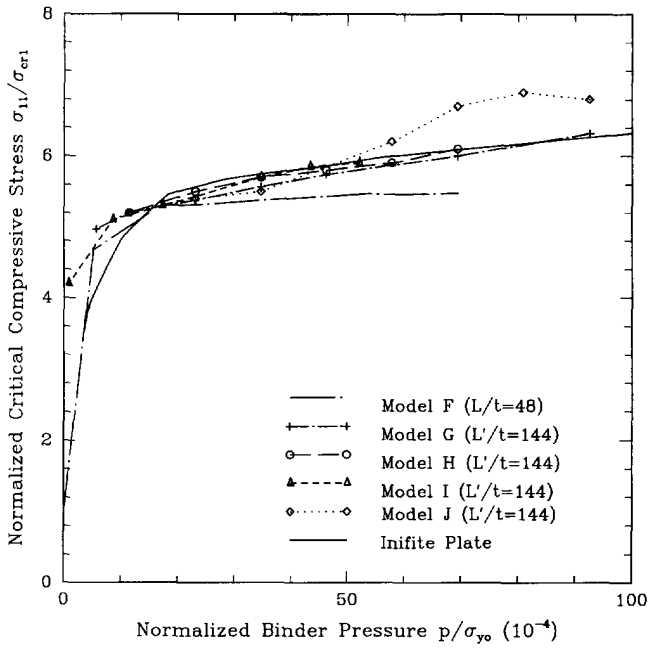

Fig. 24. Calculated and simulated critical buckling stress as a function of applied binder pressure for an elastic-plastic plate.

imperfection than to the material imperfection. For the elastic-plastic plate, the solution is insensitive to the distribution of the imperfections.

In the case where wrinkling under the binder is absolutely intolerable, that is, wrinkling must always be suppressed, one can eliminate the necessity of highly refined meshes in three-dimensional simulation by calculating the critical buckling stress as a function of applied normal pressure in advance and simply maintaining the required binder pressure depending on the compressive stress state. On the other hand, in the case where post-buckling behavior is tolerable but must be monitored, especially with respect to its influences on part shape, one can hold confidence in predicting the behavior by using a random distribution of thinned plus offset elements and/or adapting the mesh density by calculating the wavelength as a function of applied lateral pressure for that particular material. The proposed technique eliminates the need for an eigenvalue analysis to determine buckling initiation and also the need to adjust the mesh for post-buckling behavior. The method of building a robust numerical model for predicting the wrinkling behavior (onset and post-buckling) has been used in simulations of a cup drawing process where wrinkling is considered as one of the two major in-process failure modes (wrinkling and tearing). The model has been further utilized to optimize and control the forming process to enhance the performance. Preliminary results of that study were reported in Cao and Boyce (1994). More details of these applications will be demonstrated in an upcoming paper (Cao and Boyce, 1995).

Acknowledgements—This work was supported by the National Science Foundation through a PYI Award to MCB (No. DDM-9157899) and matching funds from ALCOA. We also acknowledge helpful discussions with Professor J. W. Hutchinson.

REFERENCES

ABAQUS Manual Version 5.4 (1994) Hibbitt, Karlsson & Sorensen, Inc.

Argon, A. S., Gupta, V., Landis, H. S. and Cornie, J. A. (1989). Intrinsic toughness of interfaces between SiC coatings and substrates of Si or C fiber. *J. Mater. Sci.* **24,** 1207–1218.

Cao, J. and Boyce, M. (1994). Design and control of forming parameters using finite element analysis. In *Symposium on Computational Material Modeling, ASME*, Chicago, IL, p. 265.

Cao, J. (1995). Design and control of forming parameters for sheet metal forming using finite element analysis. Ph.D thesis, MIT, Massachusetts, U.S.A.

Cao, J. and Boyce, M. (1996). A predictive tool for delaying wrinkling and tearing failures in cup forming. Submitted to J. Engng Mat. and Tech.

Cox, H. L. (1934). Buckling of thin plates in compression. *Aeron. Res. Commun., R. and M.* 1554.

Elishakoff, I. and Cai, G. Q. (1994). Non-linear buckling of a column with initial imperfection via stochastic and non-stochastic convex models. *Int. J. Non-linear Mech.* **29,** 71–82.

Fatnassi, A., Tomita, Y. and Shindo, A. (1985). Non-axisymmetric buckling behavior of elastic-plastic circular tubes subjected to a nosing operation. *Int. J. Mech. Sci.* **27,** 643–651.

Karman, Th. Von. and Tsien, H. S. (1941). The buckling of thin cylindrical shells under axial compression. *J. Aero. Sci.* **8,** 303.

Koiter, W. T. (1945). On the stability of elastic equilibrium. Thesis, Delft, H. J. Paris, Amsterdam.

Hartog, J. P. Den. (1952). *Advanced Strength of Materials*, New York, McGraw-Hill.

Hill, R. (1958). A general theory of uniqueness and stability in elastic/plastic solids. *J. Mech. Phys. Solids* **6,** 236–249.

Hutchinson, J. W. and Koiter, W. T. (1970). Post-buckling thoery. *Appl. Mech. Rev.* 1353–1366.

Hutchinson, J. W., Tennyson, R. C. and Muggeridge, D. B. (1970). Effect of a local axisymmetric imperfection on the buckling behavior of a circular cylindrical shell under axial compression. *AIAA J.* **9,** 48–52.

Hutchinson, J. W. (1974). Plastic buckling. *Adv. Appl. Mech.* **14,** 67–144.

Hutchinson, J. W. and Neale, K. W. (1985). Wrinkling of curved thin sheet metal. In *Plastic Instability*, Presses Ponts et Chaussées, Paris, pp. 71–78.

Jalkh, P., Cao, J., Hardt, D. and Boyce, M. C. (1993). Optimal forming of aluminium 2008-T4 conical cups using force trajectory control. In *Sheet Metal and Stamping Symposium*, SAE, Warrendale, PA, pp. 101–112.

Marguerre, K. and Trefftz, E. (1937). Uber die trajfahigkeit eines langsbelasteten platten-streifens nach. Uberschreiten der beullast. *Zeitschr. Angew. Math. Mech.* **17,** 121–128.

Needleman, A. (1975). Post-bifurcation behavior and imperfection sensitivity of elastic-plastic circular plates. *Int. J. Mech. Sci.* **17,** 1–13.

NumiForm, (1992). *Numerical Methods in Industrial Forming Processes*, A. A. Balkeman, Rotterdam, Netherlands.

Numisheet (1993). *Numerical Simulation of 3-D sheet Metal Forming Processes*, Makinouchi, Tokyo, Japan.

Senior, B. W. (1956). Flange wrinkling in deep-drawing operations. *J. Mech. Phys. Solids* **4,** 235–246.

Shahwan, K. W. and Waas, A. M. (1994). A mechanical model for the buckling of unilaterally constrained rectangular plates. *Int. J. Solids Structures* **31,** 75–87.

Tennyson, R. C., Muggeridge, D. B. and Caswell, R. D. (1970). The effect of axisymmetric imperfection distributions on the buckling of circular cylindrical shells under axial compression. In *AIAA/ASME 11th Structures, Structural Dynamics, and Materials Conference*, Denver, Colorado, April.

Timoshenko, S. (1961). *Theory of Elastic Stability*, New York, McGraw-Hill.

Triantafyllidis, N. and Needleman, A. (1980). An analysis of wrinkling in the swift cup test. *J. Engng Mat. Tech.* **102,** 241–248.

Tomita, Yoshihiro (1994). Simulations of plastic instabilities in solid mechanics. *Appl. Mech. Rev.* **47,** 171–205.

Wagner, H. (1929). Ebene blechwandtrager mit sehr dunnem stegblech. *Zeitschr. Flutechn. Motorluftschiffahrt* **20,** 200–306.